Journal of Alloys and Compounds 859 (2021) 157776

Contents lists available at ScienceDirect

Journal of Alloys and Compounds

journal homepage: http://www.elsevier.com/locate/jalcom

Genesis of magnetism in graphene/MoS_2 van der Waals heterostructures via interface engineering using Cr-adsorption

Renu Singla [a], Sarvesh Kumar [b], Timothy A. Hackett [c], Ali H. Reshak [d, e, f], Manish K. Kashyap [a, *]

[a] Department of Physics, Kurukshetra University, Kurukshetra, 136119, Haryana, India
[b] Inter-University Accelerator Centre (IUAC), Aruna Asaf Ali Marg, New Delhi, 110067, India
[c] Department of Biochemistry, University of Nebraska-Lincoln, Lincoln, NE, 68588-0664, USA
[d] Physics Department, College of Science, University of Basrah, Basrah, Iraq
[e] Department of Instrumentation and Control Engineering, Faculty of Mechanical Engineering, CTU in Prague, Technicka 4, Prague 6, 166 07, Czech Republic
[f] Center of Excellence Geopolymer and Green Technology, School of Material Engineering, University Malaysia Perlis, 01007, Kangar, Perlis, Malaysia

ARTICLE INFO

Article history:
Received 2 September 2020
Received in revised form
27 October 2020
Accepted 29 October 2020
Available online 4 November 2020

Keywords:
DFT
Nanomagnetism
2D heterostructure
Graphene
MoS_2

ABSTRACT

Graphene/MoS_2 heterostructure (G/MS-H) has distinctive and superlative electronic properties as it contains features of both graphene and MoS_2. Our first-principles calculations reveal this heterostructure has a little bandgap (40 meV) and zero magnetic moment in the pristine form. In the present work, we have attempted to induce magnetism in the resultant heterostructure by adsorbing Cr atom at (i) Top (G-Top) (ii) Hollow (G-Hollow) configurations in the graphene layer and (iii) Top (S-Top) and (iv) Hollow (S-Hollow) in the MoS_2 layer. However, only G-Top and S-Hollow are energetically favorable amid these configurations. Our results demonstrate that Cr-adsorption persuades the significant magnetic moment. Both the stable configurations (G-Top and S-Hollow) transpire metallicity with a Dirac point shift in the valence band. The magnetism originates from the interactions between Cr-3d states with C-2p and S-3p states. These results summarize that the resultant adsorbed heterostructure may serve as a phenomenal breakthrough for nanomagnetism.

1. Introduction

The latest progression and development in the research of novel 2D materials have opened up new avenues for the fabrication of very thin structures (in the range of nm) with restrained properties. The first member of this family is graphene, a 2D analog of carbon allotrope, graphite, and was synthesized in 2004 at the University of Manchester [1]. Graphene has several peculiar properties which proved its worth in almost all areas especially in photonics, electronics, electrochemistry, optoelectronics, and photovoltaics [2–10]. Aside from tremendous applications, graphene has some shortcomings as well. It reserves zero bandgap and zero magnetic moment in a pristine form which limit its application to optoelectronics and spintronics [11–14]. Previous theoretical and experimental studies showed the electronic and magnetic properties of graphene can be tackled easily by utilizing diverse substrates [15–21], chemical functionalization [22–27], forming nanoribbions [28,29], and with defects (tacking adatom, dopants and creating vacancies) [30–35].

The next popular members of 2D family that grabbed immense attention in their court is transition metal dichalcogenides (TMDs). TMDs form hexagonal lattice-like graphene and are represented as MX_2 where M represents a transition metal element from group IV to VI and X is a chalcogen element (S, Se, and Te). Unlike graphene, MoS_2 is a direct bandgap semiconductor with a handful of interesting and superlative optical, electronic, and mechanical properties [36–40]. Also, over time, as fabrication techniques improved, the era of van der Waals heterostructures speedily came into existence. These heterostructures are made up of the layering of different 2D materials like stacking Lego bricks in a precisely chosen sequence. In this way, many recent experimental and theoretical research in this area have shown that making heterostructure is an efficient way to

* Corresponding author.
E-mail addresses: manishdft@gmail.com, mkumar@kuk.ac.in (M.K. Kashyap).

https://doi.org/10.1016/j.jallcom.2020.157776
0925-8388/

combine the applications of two distinct 2D materials in one material and the latest attention in this area is graphene/MoS_2 heterostructure (G/MS-H). The strong spin-orbit coupling (SOC) of MoS_2 with C atom leads to the opening of a bandgap in graphene at the Dirac point [41]. The extraordinary features of G/MS-H like strong optical response with high quantum efficiency, exceptional photoconductivity, and generation of large photocurrent have already led to the construction of nanosensors, optical switches, energy storage devices, and logic gates [42–53]. But the simulation of this G/MS-H by density functional theory (DFT) is at the expense of quite high computational cost and very challenging due to van der Waals (vdw) interactions and large mismatch in lattice between the layers. Various strives were made by researchers to seek out the problem of lattice mismatch, choice of proper vdw functional, accurate interlayer spacing, and charge transfer between the layers. Finally, Singh et al. [54] resolved all these problems theoretically by presenting a comparative study of different DFT vdW methods for 5×5:4×4 and 4×4:3×3 geometries of graphene/MoS_2. They revealed that DFT-TS and DFT-D2 methods measure accurately interlayer spacing (3.40 Å). The Dirac point is located near the conduction band of MoS_2 sheet for 4×4:3×3 and lies in the bandgap region for 5×5:4×4 geometry, leading to appreciable charge transfer in the former and no charge transfer between the constituent layers in the later. The zero magnetic moment of G/MS-H limits its potential worth in magnetism. The previous papers from various research groups [55–58] showed that significant magnetic moment can be induced in the bilayer graphene by doping a transition metal atom (Fe, Cr, and Mn) in three different locations (Top, Hollow and Bottom) and the resultant systems become highly promising in spintronic and memory-based devices. This motivated us to induce the magnetic moment in G/MS-H in a similar way by adsorbing a suitable transition metal atom. Thus, we focus on the comprehensive theoretical study of Cr-adsorption in both the upper and lower layers of G/MS-H separately. The selection of Cr atom is made due to its large magnetic moment of 6 μ_B in the free-standing form which may result high induced moment on G/MS-H after adsorption.

2. Computational details

The *ab-initio* calculations were performed in VASP that utilize a plane-wave basis approach based on density functional theory (DFT) [59,60]. The generalized gradient approximation (GGA) within Perdew-Burke-Ernzerhof (PBE) functional was employed to address the electron-electron exchange-correlation (XC) potentials [61]. The difficulties in lattice mismatch between graphene and MoS_2 layer was addressed with $5 \times 5 \times 1$ supercell of graphene and $4 \times 4 \times 1$ supercell of MoS_2. The periodic interactions between the layers were avoided by inserting a vacuum layer of thickness 20 Å. Also, vdW interactions were incorporated in the resultant heterostructure with the help of DFT-D2 method of Grimme [62]. To optimize the internal coordinates of atoms and lattice parameters, the conjugate gradient algorithm (CG) was adopted under tight convergence criteria of 10^{-8} eV. We sat the maximum plane-wave energy cut off as 520 eV and the Brillouin zone was sampled with Γ-type k-points mesh of $6 \times 6 \times 1$. The SOC was also included to better understand the intrinsic coupling in the resultant heterostructures. The vibrational stability of the resultant heterostructure was checked within a density functional perturbation theory (DFPT) approach by performing the phonon spectrum. The data was further processed with the help of phonopy code [63]. Also, the stability against thermal fluctuations at 300 K was measured with the help of *ab-initio* molecular dynamics simulations (AIMD) [64]. The charge redistribution and charge transfer between the layers were predicted by using Bader charge analysis [65].

3. Results and discussions

3.1. Pristine graphene/MoS_2 heterostructure

Since the lattice constant of graphene (2.456 Å) and MoS_2 (3.169 Å) are quite different, therefore, first of all, the lattice mismatch was compensated by assembling $5 \times 5 \times 1$ supercell of graphene with $4 \times 4 \times 1$ supercell of MoS_2 (Fig. 1). The observed lattice parameters of relaxed pristine 5:4 bilayer heterostructure are $a = b = 12.41$ Å. The bond lengths of Mo–S and C–C were found to be 2.4 Å and 1.48 Å, respectively. Also, the thickness of the MoS_2 layer, i.e., the distance between S–S planes, is 3.16 Å and interlayer spacing (d) between graphene and MoS_2 layers is 3.42 Å. Both these values agree with the calculated values of Singh et al. [60]. After that, Cr atom is adsorbed at all possible configurations i.e. Top, Hollow, and Bottom in both the layers. As graphene layer is a single atom thick (C), so, it has three favorable locations for Cr-adsorption i.e. G-Top (top of any C atom directly), G-Hollow (center of hexagon of C atoms), G-Bottom (at the midpoint of C–C bond). But the MoS_2 layer is three atoms thick (one Mo and two S). So, it has six favorable locations i.e. S-Top (top of any S atom directly), Mo-Top (top of any Mo atom directly), S-Hollow & Mo-Hollow (center of hexagon of Mo and S atoms), S-Bottom & Mo-Bottom (at the midpoint of Mo–S bond). It is worth to mention here that (i) Mo-Hollow and S-Hollow as well as (ii) Mo-Bottom and S-Bottom are equivalent configurations. This means there are seven possible configurations in which Cr-adsorption is possible. However, out of these seven, three configurations *viz.* G-Bottom, Mo-Top, S-Bottom are not stable and transform to G-Top, S-Hollow, and S-Hollow, respectively. Therefore, we proceed further only with rest of the four configurations as depicted in Fig. 1.

We primarily computed the structural stability of pristine and all four adsorbed heterostructures by estimating binding energy [57,66] as:

$$\begin{aligned} E_{bin} &= E_{prist} - n_l E_{MoS_2} - n_l E_{Graphene} \text{ (For pristine case)} \\ &= E_{adsorbed} - n_l E_{MoS_2} - n_l E_{Graphene} - n_{Cr} E_{Cr} \text{ (For adsorbed case)} \end{aligned} \quad (1)$$

where $E_{prist}/E_{adsorbed} E_{MoS_2}, E_{Graphene}$ and E_{Cr} are the ground state energies of pristine/adsorbed heterostructures, MoS_2 monolayer, graphene monolayer, and Cr atom, respectively. Also, n_l represents the number of layers of MoS_2 and graphene and n_{Cr} represents the number of Cr atoms in the resultant heterostructures.

Table 1 is indicative that there is a negligible difference between interlayer spacing and thickness of MoS_2 layer of pristine and all adsorption cases. This may be due to the fact that the electronegativity of Cr atom is less than both C and S atoms due to which it does not cause any strain on both graphene and MoS_2 layers, leaving '*d*' and '*t*' almost intact. Also, it is clearly reflected from the binding energy values (Table 1) that only pristine case along with G-Top and S-Hollow are energetically favorable. Thus, we have considered only these three configurations for further detailed investigation of the electronic properties and magnetic response. The stability of the pristine case under thermal fluctuations at about 300 K is also determined with the help of AIMD simulations. The result shows that total energy is varied minutely with a time step of 200 fs (Fig. 2). In addition, no movements and breaking of bonds between the atoms in the corresponding monolayers were observed, indicating the thermal stability of the resultant heterostructure.

In addition, vibrational stability was also ensured with the help of the phonon spectrum. The phonon dispersion spectrum contains mostly positive frequencies except only one or two negatives values

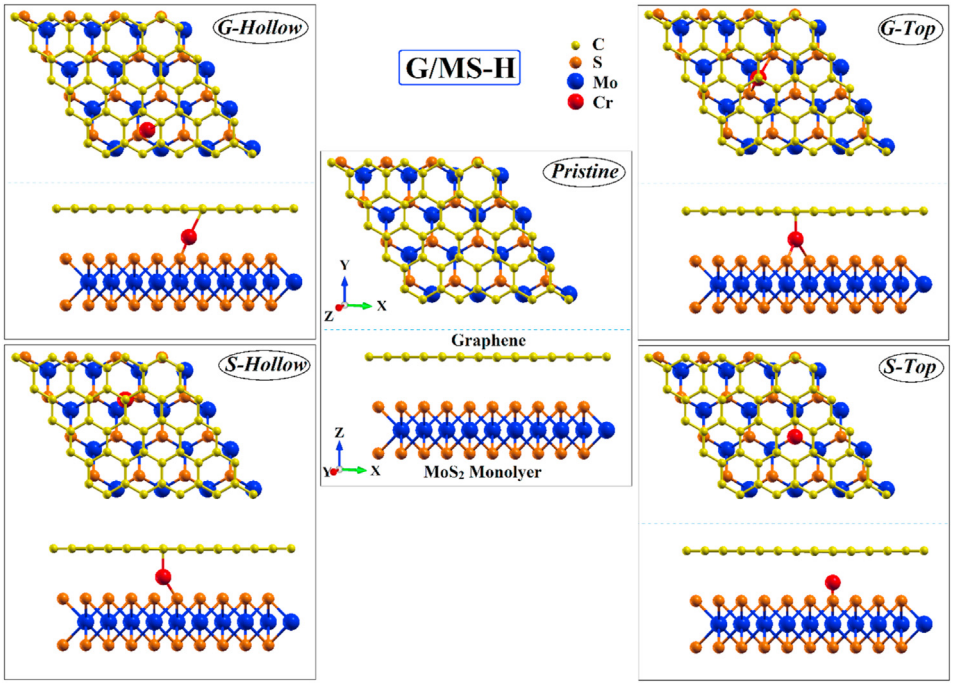

Fig. 1. Schematics of 5:4 vdW G/MS-H in pristine form (middle) and after Cr-adsorption in Hollow (left) and Top (right) configurations.

Table 1
Optimized lattice parameters, interlayer spacing (d) between graphene and MoS_2 layer, thickness (t) of MoS_2 layer and binding Energy (E_{bin}) of pristine and Cr-adsorbed G/MS-H.

Parameters	Pristine	G-Hollow	G-Top	S-Hollow	S-Top
Lattice parameters	a = b = 12.41	a = b = 12.42	a = b = 12.43	a = b = 12.43	a = b = 12.43
a,b,c (Å)	c = 22.51	c = 22.52	c = 22.48	c = 22.47	c = 22.49
d (Å)	3.423	3.419	3.411	3.412	3.415
t (Å)	3.16	3.15	3.13	3.14	3.14
E_{bin} (eV)	−0.62	+0.53	−1.45	−0.87	+1.70

at Γ-point (Fig. 3) which generally arise in 2D materials due to the absence of the substrate.

The spin-resolved band structure of pristine G/MS-H (Fig. 4) demonstrates the mirror-like symmetry only in the proximity of the Fermi level (E_F), resembling pristine graphene with an exception of a direct bandgap of about 40 meV at K-point of Irreducible Brillouin Zone (IBZ). Also, the band structure for the majority and minority spin channels are exactly similar. This manifests that

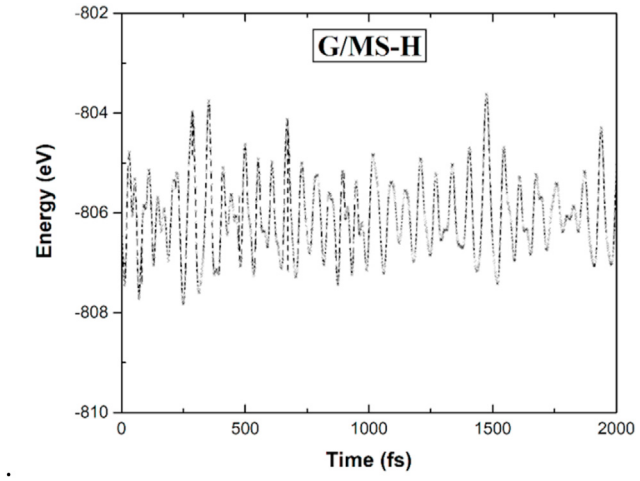

Fig. 2. Thermal fluctuations in the total energy of pristine G/MS-H at room temperature (300 K) as governed by AIMD simulations.

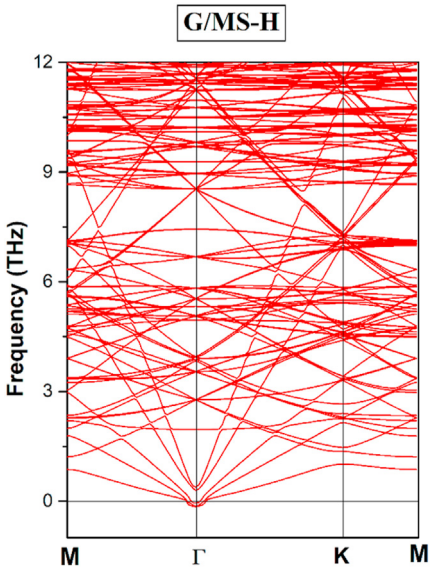

Fig. 3. Phonon dispersion spectrum for pristine G/MS-H along high symmetry k-points.

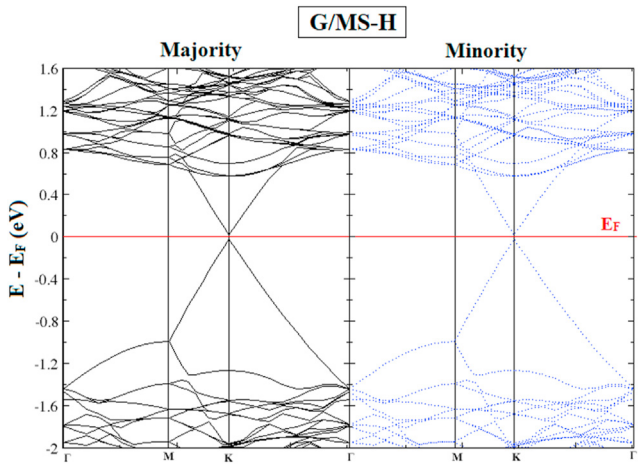

Fig. 4. Spin resolved band structure of pristine G/MS-H in majority and minority spin channel.

pristine G/MS-H has zero magnetic moment which limits its potential in nanomagnetism.

To better understand the opening of the gap between Dirac points, the charge transfer, and changes in electronic structures of resultant G/MS-H due to vdW interactions between graphene and MoS_2 layers, the total and orbital projected density of states (DOS) for pristine graphene monolayer, pristine MoS_2 monolayer and pristine G/MS-H are analyzed in Fig. 5.

In G/MS-H, the electronic bands forming the Dirac cone in environs of E_F are mainly composed of C-2*p* states whereas, the valence and conduction bands away from the E_F are dominated by S-3p and Mo-4d states. Also, when the orbital character of C/(Mo and S) in graphene/(MoS_2) monolayer only (Fig. 5) are compared with the corresponding orbital characters in G/MS-H (Fig. 5), it is found that the orbital characters of Mo (4d) and S (3p) in MoS_2 and C (2p) in graphene monolayer are almost intact as in G/MS-H which indicate a zero charge transfer between the corresponding layers. Despite this zero charge transfer, there are some significant changes at the Dirac point of the resultant heterostructure as compared to the individual graphene monolayer. In addition to some bandgap between the Dirac points, the shape of the Dirac cone is changed to somewhat parabolic instead of linear as in graphene. Also, in an individual MoS_2 monolayer, the valence band is filled close to E_F whereas in G/MS-H, the valence band of these Mo-d and S-p orbitals is far left from the E_F. These effects may originate due to the effective staggered potential arising from MoS_2 and competition between the intrinsic SOC of graphene with MoS_2.

The zero charge transfer between the corresponding layers under equilibrium conditions was further verified with the help of Bader charge analysis. The electronegativity of both Mo and S atoms are different due to which each S atom accepts 0.58e from Mo atom. In other words, each Mo atom donates 1.16e as MoS_2 layer has two S atoms per Mo atom. However, in the graphene layer, there is zero charge transfer as electronegativities of all C atoms are the same. When graphene and MoS_2 are combined together in the heterostructure, even then S atom accepts 0.58 e from Mo atom and there is no charge transferred to the C atom. This clearly indicates that there is no trace of charge transfer from Mo/S atom to C atom and vice versa in the resultant heterostructure (Table 2).

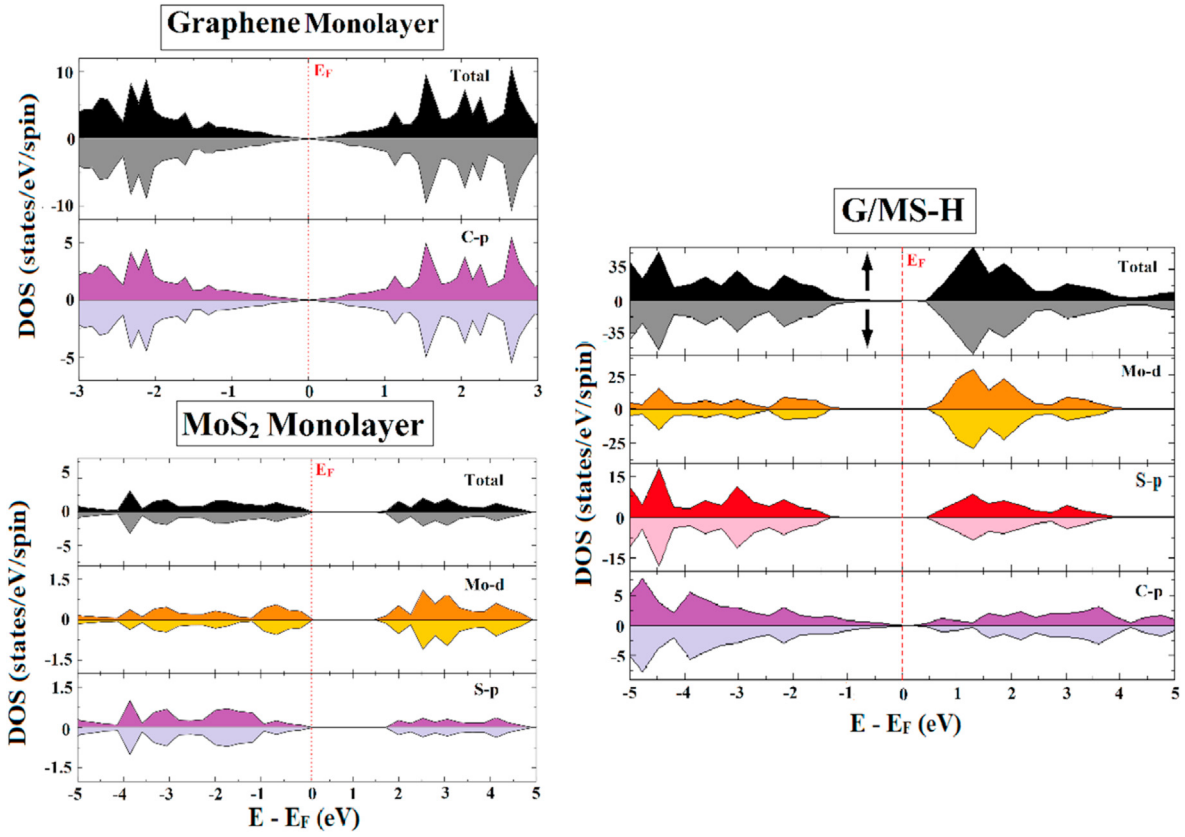

Fig. 5. Calculated spin-resolved total and partial DOS of pristine Graphene Monolayer, MoS_2 Monolayer and G/MS-H. E_F is shifted to zero.

Table 2
Calculated average charge transfer by Mo, S, and C atoms between the MoS_2 and graphene monolayers in G/MS-H.

Atoms	Charge transfer G/MS-H (in electrons)	Charge transfer Graphene Monolayer (in electrons)	Charge transfer MoS_2 Monolayer (in electrons)
Mo	+1.16 e	_	+1.16 e
S	−0.58 e	_	−0.58 e
C	−0.02 e	−0.02 e	_

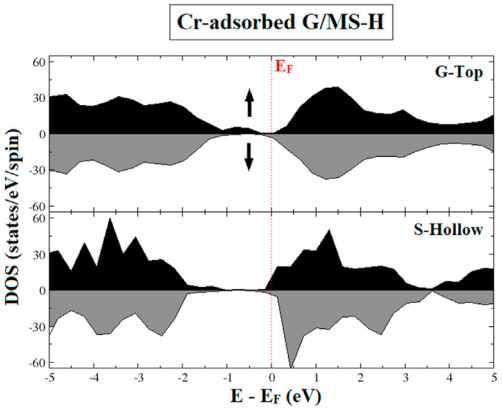

Fig. 6. Calculated spin-resolved total DOS for Cr-adsorbed G/MS-H in G-Top and S-Hollow configurations.

3.2. Cr-adsorbed G/MS-H

The Cr atom highly influences the electronic and magnetic properties of resultant G/MS-H and leads to the modification in the total DOS for both configurations, as delineated in Fig. 6, reflecting the disappearance of the feeble gap of the pristine case due to the adoption of E_F by DOS of adsorbed Cr-atom. Clearly, in Cr-adsorbed G/MS-H, the valence and conduction bands overlap with each other and the overlapping bands pilot the passage of heterostructure from low bandgap semiconductor to the metal for both configurations. Moreover, the presence of Cr atom not only leads to the addition of extra states in the vicinity of E_F but also alters the orbital projected DOS of Mo-4d and S-3p (Fig. 7). Now, the unoccupied DOS (in conduction band) of both Mo-4d and S-3p orbitals touch E_F whereas in pristine G/MS-H, they remain present well above the E_F. Also, the location of the adsorption site is very crucial as DOS is different for both G-Top and S-Hollow.

The slight differences between the DOS of G-Top and S-Hollow are due to the fact that the electronegativity of the S atom is slightly higher than that of C atom. As a result of which, it tends to attract more electron cloud from Cr-3d orbitals. In both G-Top and S-Hollow configurations, metal character arises mainly due to admixture of 2p/3p orbitals of C/S with 3d orbitals of Cr atom (Fig. 7). Also, both the configurations have decent magnetic moments (as listed in Table 3) which make the resultant heterostructures the phenomenal candidates for various magnetic applications such as memory-based magnetic devices and spintronics.

This appearance of significant magnetic moment and alteration in DOS on adsorption can be better understood with the help of

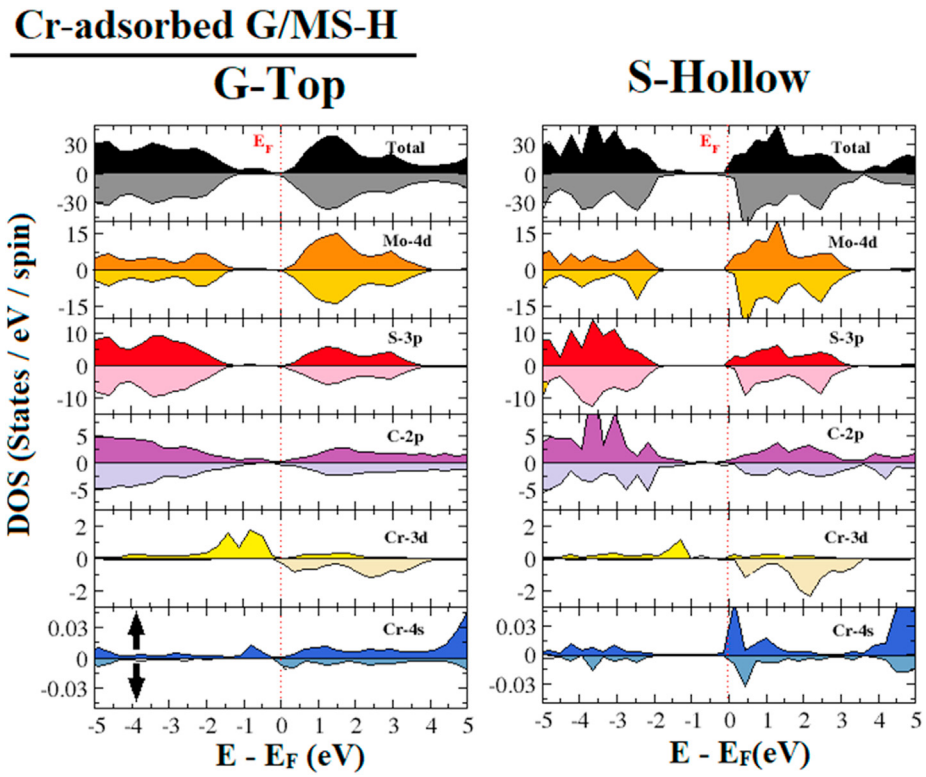

Fig. 7. Orbital projected spin-resolved DOS of G/MS-H in G-Top and S-Hollow configurations.

Table 3
Total spin Magnetic moments μ_{stot} (μ_B) and the amount of charge transfer for Cr-adsorbed G/MS-H.

Property	Configuration			
	G-Top		S-Hollow	
μ_{stot}	3.748		3.436	
Amount of charge Transfer	Cr	=+0.99 e	Cr	=+1.05 e
	C_{neigh}	=−0.19 e	S_{neigh}	=−0.77 e
	C_{far}	=0	S_{far}	=−0.58 e
	Mo_{neigh}	=+1.14 e	Mo_{neigh}	=+1.13 e
	Mo_{far}	=+1.16 e	Mo_{far}	=+1.16 e
	S_{neigh}	=−0.72 e	C_{neigh}	=−0.12 e
	S_{far}	=−0.58 e	C_{far}	=0

charge transfer using Bader charge analysis. It is clearly reflected from Table 3 that the charge transfer is affected only for those Mo, C, and S atoms which are in the vicinity of Cr atom while the remaining atoms which are far away from the adsorption site, have the same charge transfer as that in pristine case. In G-Top/S-Hollow, C/S atoms are closer to Cr atoms than S/C atoms. As a result, the C atoms withdraw more electrons from Cr atom in G-Top and S atoms withdraw more electrons from Cr atom in S-Hollow with respect to each other. Also, Cr atom loses more electrons in S-Hollow than G-Top because the electronegativity of S atom is slightly higher than that of C atom.

The spin magnetic moment in G-Top/S-Hollow appears only due to Cr atom itself. The spin magnetic moment of the Cr atom ($3d^5 4s^1$) should be 6 μ_B in its free-standing form. However, the total spin magnetic moment (μ_{stot}) of G-Top/S-Hollow comes out to be 3.748/3.436 μ_B. This reduction in the magnetic moment takes place due to the shifting of electrons from 3d to 4s orbitals of Cr atom to the S-3p and C-2p orbitals. Also, the greater the shifting of electrons, the more will be the reduction in the magnetic moment. Clearly, the chance of shifting of electrons from Cr atom is more in S-Hollow than G-Top (Table 3) configuration. That is why, the magnetic moment of S-Hollow is less than that of G-Top. In addition, we have checked the variation in magnetic moment in ab-plane and perpendicular to the heterostructure. But no significant change is appeared, indicating no role of direction dependence. Thus, in a nutshell, we can conclude the variation between orbital projected DOS and magnetic moments for both configurations are the consequence of different charge transfer in both cases.

The magnetic character induced by Cr atom is cross-verified by plotting spin density plots of both graphene and MoS_2 monolayer in S-Hollow Cr adsorbed G/MS-H (Fig. 8). These plots illustrate that the main contribution to the magnetic moment arises from the Cr atom. Also, it influences the spin states of only those S atoms of MoS_2 layer and C atoms of graphene layer which lies in its proximity while the spin states of remaining atoms of both layers remain the same as before adsorption. A similar behavior is observed (not shown for brevity) for G-Top configuration of the studied heterostructure.

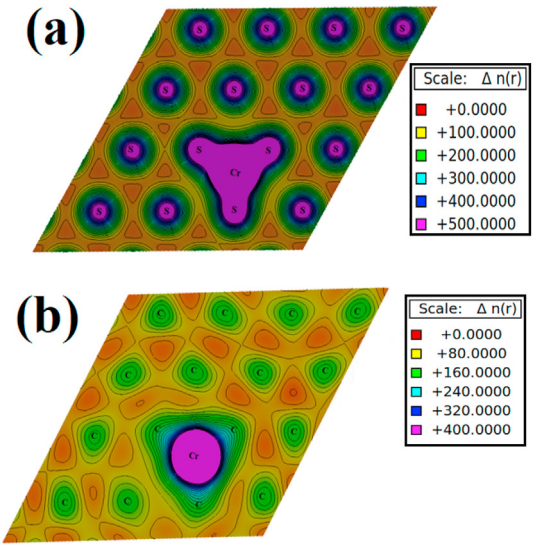

Fig. 8. Spin density profile in (a) MoS_2 monolayer and b) Graphene monolayer along 110 plane of G/MS-H with S-Hollow configuration.

4. Conclusions

In summary, the electronic and magnetic response of pristine as well as Cr-adsorbed graphene/MoS_2 heterostructure in various configurations have been studied within the framework of density functional theory. Our results present that Cr-adsorption leads to the transition of pristine heterostructure from weak semiconductor to the metal and introduces the significant magnetic moment in both the stable configurations. The bonding of the Cr atom with nearest S atoms in the MoS_2 layer and C atoms in the graphene layer is covalent as evident from the Bader charge analysis. This covalent bonding reduces the magnetic moment of the Cr atom in comparison to its free-standing state. Also, the slight difference between the magnetic moment and electronic DOS of both the configurations is due to the difference in electronegativities of C and S atoms. These results summarize that the resultant adsorbed heterostructure can be an efficient candidate for nano-magnetic devices.

CRediT authorship contribution statement

Renu Singla: Investigation, Software, Data curation, Validation, Visualization, Writing - original draft. **Sarvesh Kumar:** Visualization, Writing - review & editing, Formal analysis. **Timothy A. Hackett:** Visualization, Writing - original draft, Writing - review & editing. **Ali H. Reshak:** Methodology, Writing - review & editing, Formal analysis. **Manish K. Kashyap:** Conceptualization, Methodology, Supervision, Writing - review & editing, Formal analysis, Project administration, Funding acquisition, All authors contributed to the discussion.

Declaration of competing interest

The authors declare that they have no known competing financial interests or personal relationships that could have appeared to influence the work reported in this paper.

Acknowledgments

The computation in this work was performed using Param Shavak supercomputing machine available at Department of Physics, Kurukshetra University, Kurukshetra (Haryana), and the National PARAM Supercomputing Facility (NPSF) of Centre for Development of Advanced Computing (C-DAC), Pune, India. R.S. would like to acknowledge the financial support from Council of Scientific & Industrial Research (CSIR), New Delhi (India) in the form of a junior research fellowship (JRF). M. K. Kashyap acknowledges DST-SERB, New Delhi, India for providing financial assistantship vide grant no. EMR/2016/007380.

References

[1] A.K. Geim, K.S. Novoselov, The Rise of Graphene, Nanoscience and Technology: a Collection of Reviews from Nature Journals, 2010, pp. 11–19.
[2] A.K. Geim, I.V. Grigorieva, Van der Waals heterostructures, Nature 499 (7459) (2013) 419–425.
[3] A.A. Balandin, S. Ghosh, W. Bao, I. Calizo, D. Teweldebrhan, F. Miao, C.N. Lau, Superior thermal conductivity of single-layer graphene, Nano Lett. 8 (3) (2008) 902–907.
[4] A.K. Geim, Graphene: status and prospects, Science 324 (5934) (2009) 1530–1534.
[5] A.S. Mayorov, R.V. Gorbachev, S.V. Morozov, L. Britnell, R. Jalil, L.A. Ponomarenko, P. Blake, K.S. Novoselov, K. Watanabe, T. Taniguchi, A.K. Geim, Micrometer-scale ballistic transport in encapsulated graphene at room temperature, Nano Lett. 11 (6) (2011) 2396–2399.
[6] K.I. Bolotin, K.J. Sikes, J. Hone, H.L. Stormer, P. Kim, Temperature-dependent transport in suspended graphene, Phys. Rev. Lett. 101 (9) (2008), 096802.
[7] Z. Chen, Y.M. Lin, M.J. Rooks, P. Avouris, Graphene nano-ribbon electronics, Phys. E Low-dimens. Syst. Nanostruct. 40 (2) (2007) 228–232.
[8] C. Lee, X. Wei, J.W. Kysar, J. Hone, Measurement of the elastic properties and intrinsic strength of monolayer graphene, Science 321 (5887) (2008) 385–388.
[9] K.S. Novoselov, V.I. Fal, L. Colombo, P.R. Gellert, M.G. Schwab, K. Kim, A roadmap for graphene, Nature 490 (7419) (2012) 192–200.
[10] L. Sun, Q. Li, H. Ren, H. Su, Q.W. Shi, J. Yang, Strain effect on electronic structures of graphene nanoribbons: a first-principles study, J. Chem. Phys. 129 (7) (2008), 074704.
[11] D. Van Tuan, F. Ortmann, A.W. Cummings, D. Soriano, S. Roche, Spin dynamics and relaxation in graphene dictated by electron-hole puddles, Sci. Rep. 6 (2016) 21046.
[12] B. Dlubak, M.B. Martin, C. Deranlot, B. Servet, S. Xavier, R. Mattana, M. Sprinkle, C. Berger, W.A. Deer, F. Petroff, A. Anane, P. Seneor, A. Fert, Highly efficient spin transport in epitaxial graphene on SiC, Nat. Phys. 8 (7) (2012) 557–561.
[13] A.W. Cummings, S. Roche, Effects of dephasing on spin lifetime in ballistic spin-orbit materials, Phys. Rev. Lett. 116 (8) (2016), 086602.
[14] M. Drögeler, C. Franzen, F. Volmer, T. Pohlmann, L. Banszerus, M. Wolter, K. Watanable, T. Taniguchi, C. Stampfer, B. Beschoten, Spin lifetimes exceeding 12ns in graphene nonlocal spin valve devices, Nano Lett. 16 (6) (2016) 3533–3539.
[15] F. Varchon, R. Feng, J. Hass, X. Li, B.N. Nguyen, C. Naud, P. Mallet, J.Y. Veuillen, C. Berger, E.H. Conrad, L. Magaud, Electronic structure of epitaxial graphene layers on SiC: effect of the substrate, Phys. Rev. Lett. 99 (12) (2007) 126805.
[16] R. Decker, Y. Wang, V.W. Brar, W. Regan, H.Z. Tsai, Q. Wu, W. Gannett, A. Zettl, M.F. Crommie, Local electronic properties of graphene on a BN substrate via scanning tunneling microscopy, Nano Lett. 11 (6) (2011) 2291–2295.
[17] T.C. Nguyen, M. Otani, S. Okada, Semiconducting electronic property of graphene adsorbed on (0001) surfaces of SiO_2, Phys. Rev. Lett. 106 (10) (2011) 106801.
[18] Z. Wang, C. Tang, R. Sachs, Y. Barlas, J. Shi, Proximity-induced ferromagnetism in graphene revealed by the anomalous Hall effect, Phys. Rev. Lett. 114 (1) (2015), 016603.
[19] H.X. Yang, A. Hallal, D. Terrade, X. Waintal, S. Roche, M. Chshiev, Proximity effects induced in graphene by magnetic insulators: first-principles calculations on spin filtering and exchange-splitting gaps, Phys. Rev. Lett. 110 (4) (2013), 046603.
[20] A. Barla, V. Bellini, S. Rusponi, P. Ferriani, M. Pivetta, F. Donati, F. Patthey, L. Persichetti, S.K. Mahatha, M. Papagno, C. Piamonteze, S. Fitchner, S. Heinze, P. Gambardella, H. Brune, C. carbone, Complex magnetic exchange coupling between co nanostructures and Ni (111) across epitaxial graphene, ACS Nano 10 (1) (2016) 1101–1107.
[21] A. Miyashita, M. Maekawa, K. Wada, A. Kawasuso, T. Watanabe, S. Entani, S. Sakai, Spin polarization of graphene and h–BN on Co (0001) and Ni (111) observed by spin-polarized surface positronium spectroscopy, Phys. Rev. B 97 (19) (2018) 195405.
[22] T.S. Sreeprasad, V. Berry, How do the electrical properties of graphene change with its functionalization? Small 9 (3) (2013) 341–350.
[23] J.A. Yan, M.Y. Chou, Oxidation functional groups on graphene: structural and electronic properties, Phys. Rev. B 82 (12) (2010) 125403.
[24] J. Dai, J. Yuan, Adsorption of molecular oxygen on adsorbed graphene: atomic, electronic, and magnetic properties, Phys. Rev. B 81 (16) (2010) 165414.
[25] H. González-Herrero, J.M. Gómez-Rodríguez, P. Mallet, M. Moaied, J.J. Palacios, C. Salgado, M.M. Ugeda, J.Y. Veuillen, F. Yndurain, I. Brihuega, Atomic-scale control of graphene magnetism by using hydrogen atoms, Science 352 (6284) (2016) 437–441.
[26] A.V. Krasheninnikov, P.O. Lehtinen, A.S. Foster, P. Pyykkö, R.M. Nieminen, Embedding transition-metal atoms in graphene: structure, bonding, and magnetism, Phys. Rev. Lett. 102 (12) (2009) 126807.
[27] J. Nokelainen, I.V. Rozhansky, B. Barbiellini, E. Lähderanta, K. Pussi, Gate-tunable magnetism of C adatoms on graphene, Phys. Rev. B 99 (3) (2019), 035441.
[28] Y.-W. Son, M.L. Cohen, S.G. Louie, Energy gaps in graphene nanoribbons, Phys. Rev. Lett. 97 (2006) 216803.
[29] M.Y. Han, B. Özyilmaz, Y. Zhang, P. Kim, Energy band-gap engineering of graphene nanoribbons, Phys. Rev. Lett. 98 (20) (2007) 206805.
[30] L. Liu, M. Qing, Y. Wang, S. Chen, Defects in graphene: generation, healing, and their effects on the properties of graphene: a review, J. Mater. Sci. Technol. 31 (6) (2015) 599–606.
[31] A. Lopez-Bezanilla, J.L. Lado, Defect-induced magnetism and Yu-Shiba-Rusinov states in twisted bilayer graphene, Phys. Rev. Mater. 3 (8) (2019), 084003.
[32] O.V. Yazyev, L. Helm, Defect-induced magnetism in graphene, Phys. Rev. B 75 (12) (2007) 125408.
[33] Y. Ma, Y. Dai, M. Guo, B. Huang, Graphene-diamond interface: gap opening and electronic spin injection, Phys. Rev. B 85 (23) (2012) 235448.
[34] J. Červenka, M.I. Katsnelson, C.F.J. Flipse, Room-temperature ferromagnetism in graphite driven by two-dimensional networks of point defects, Nat. Phys. 5 (11) (2009) 840–844.
[35] M. Rafique, Y. Shuai, H.P. Tan, M. Hassan, Structural, electronic and magnetic properties of 3d metal trioxide clusters-adsorbed monolayer graphene: a first-principles study, Appl. Surf. Sci. 399 (2017) 20–31.
[36] J.A. Wilson, A.D. Yoffe, The transition metal dichalcogenides discussion and interpretation of the observed optical, electrical and structural properties, Adv. Phys. 18 (73) (1969) 193–335.
[37] R. Tenne, L. Margulis, M.E. Genut, G. Hodes, Polyhedral and cylindrical structures of tungsten disulphide, Nature 360 (6403) (1992) 444–446.
[38] B. Radisavljevic, A. Radenovic, J. Brivio, V. Giacometti, A. Kis, Single-layer MoS_2 transistors, Nat. Nanotechnol. 6 (3) (2011) 147–150.
[39] S. Tongay, J. Zhou, C. Ataca, K. Lo, T.S. Matthews, J. Li, J.C. Grossman, J. Wu, Thermally driven crossover from indirect toward direct bandgap in 2D semiconductors: $MoSe_2$ versus MoS_2, Nano Lett. 12 (11) (2012) 5576–5580.
[40] A. Castellanos-Gomez, M. Poot, G.A. Steele, H.S. Van Der Zant, N. Agraït, G. Rubio-Bollinger, Elastic properties of freely suspended MoS_2 nanosheets, Adv. Mater. 24 (6) (2012) 772–775.
[41] C.P. Lu, G. Li, K. Watanabe, T. Taniguchi, E.Y. Andrei, MoS_2: choice substrate for accessing and tuning the electronic properties of graphene, Phys. Rev. Lett. 113 (15) (2014) 156804.
[42] E. Lee, S.G. Lee, W.H. Lee, H.C. Lee, N.N. Nguyen, M.S. Yoo, K. Cho, Direct CVD growth of graphene/MoS_2 heterostructure with interfacial bonding for two-dimensional electronics, Chem. Mater. 32 (11) (2020) 4544–4552.
[43] X. Yu, J. Tang, K. Terabe, T. Sasaki, R. Gao, Y. Ito, K. Nakura, K. Asano, M.A. Suzuki, Fabrication of graphene/MoS_2 alternately stacked structure for enhanced lithium storage, Mater. Chem. Phys. 239 (2020) 121987.
[44] S. Subramanian, K. Xu, Y. Wang, S. Moser, N.A. Simonson, D. Deng, V.H. Crespi, S.K. Fullerton-Shirey, J.A. Robinson, Tuning transport across MoS_2/graphene interfaces via as-grown lateral heterostructures, 2D Mater. Appl. 4 (1) (2020) 1–5.
[45] K. Roy, M. Padmanabhan, S. Goswami, T.P. Sai, G. Ramalingam, S. Raghavan, A. Ghosh, Graphene–MoS_2 hybrid structures for multifunctional photoresponsive memory devices, Nat. Nanotechnol. 8 (11) (2013) 826–830.
[46] S. Bertolazzi, D. Krasnozhon, A. Kis, Nonvolatile memory cells based on MoS_2/graphene heterostructures, ACS Nano 7 (4) (2013) 3246–3252.
[47] M.S. Choi, G.H. Lee, Y.J. Yu, D.Y. Lee, S.H. Lee, P. Kim, J. Hone, W.J. Yoo, Controlled charge trapping by moly bdenumdisulphide and graphene in ultrathin heterostructured memory devices, Nat. Commun. 4 (1) (2013) 1–7.
[48] X. Yu, G. Zhao, S. Gong, C. Liu, C. Wu, P. Lyu, G. Maurin, N. Zhang, Design of MoS_2/graphene van der Waals heterostructure as highly efficient and stable electrocatalyst for hydrogen evolution in acidic and alkaline media, ACS Appl. Mater. Interfaces 12 (22) (2020) 24777–24785.
[49] S. Larentis, J.R. Tolsma, B. Fallahazad, D.C. Dillen, K. Kim, A.H. MacDonald, E. Tutuc, Band offset and negative compressibility in graphene-MoS_2 heterostructures, Nano Lett. 14 (4) (2014) 2039–2045.
[50] L. Yu, Y.H. Lee, X. Ling, E.J.G. Santos, Y.C. Shin, Y. Lin, M. Dubey, E. Kaxiras, J. Kong, H. Wang, T. Palacios, Graphene/MoS_2 hybrid technology for large-scale two-dimensional electronics, Nano Lett. 14 (6) (2014) 3055–3063.
[51] K.S. Novoselov, A. Mishchenko, A. Carvalho, A.C. Neto, 2D materials and van der Waals heterostructures, Science 353 (6298) (2016).
[52] W. Zhang, C.P. Chuu, J.K. Huang, C.H. Chen, M.L. Tsai, Y.H. Chang, M.Y. Chou, C.T. Liang, Y.Z. chen, J.H. He, L.J. Li, Ultrahigh-gain photodetectors based on atomically thin graphene-MoS_2 heterostructures, Sci. Rep. 4 (2014) 3826.
[53] D. Deng, K.S. Novoselov, Q. Fu, N. Zheng, Z. Tian, X. Bao, Catalysis with two-dimensional materials and their heterostructures, Nat. Nanotechnol. 11 (3) (2016) 218–230.
[54] S. Singh, C. Espejo, A.H. Romero, Structural, electronic, vibrational, and elastic properties of graphene/MoS_2 bilayer heterostructures, Phys. Rev. B 98 (15) (2018) 155309.
[55] Y. Mao, G.M. Stocks, J. Zhong, First-principles study of the doping effects in bilayer graphene, New J. Phys. 12 (2010), 033046.
[56] Y. Mao, J. Zhong, Structural, electronic and magnetic properties of manganese doping in the upper layer of bilayer graphene, Nanotechnology 19 (20) (2008) 205708.
[57] R. Singla, J. Thakur, P. Rani, S. Kumar, T.A. Hackett, M.K. Kashyap, Emergence of magnetic behavior in AB-stacked bilayer graphene via Fe-doping, Vacuum 182 (2020) 109685.
[58] J. Thakur, M.K. Kashyap, H.S. Saini, A.H. Reshak, Enhanced magnetic response and metallicity in AB stacked bilayer graphene via Cr-doping, J. Alloys Compd. 649 (2015) 1300–1305.
[59] G. Kresse, J. Furthmüller, Efficient iterative schemes for ab initio total-energy calculations using a plane-wave basis set, Phys. Rev. B 54 (16) (1996) 11169.

[60] G. Kresse, D. Joubert, From ultrasoft pseudopotentials to the projector augmented-wave method, Phys. Rev. B 59 (3) (1999) 1758.
[61] J.P. Perdew, K. Burke, M. Ernzerhof, Generalized gradient approximation made simple, Phys. Rev. Lett. 77 (18) (1996) 3865.
[62] S. Grimme, Semiempirical GGA-type density functional constructed with a long-range dispersion correction, J. Comput. Chem. 27 (15) (2006) 1787–1799.
[63] A. Togo, F. Oba, I. Tanaka, First-principles calculations of the ferroelastic transition between rutile-type and $CaCl_2$-type SiO_2 at high pressures, Phys. Rev. B 78 (13) (2008) 134106.
[64] M. Parrinello, A. Rahman, Crystal structure and pair potentials: a molecular-dynamics study, Phys. Rev. Lett. 45 (14) (1980) 1196.
[65] M. Yu, D.R. Trinkle, Accurate and efficient algorithm for Bader charge integration, J. Chem. Phys. 134 (6) (2011), 064111.
[66] P. Rani, M.K. Kashyap, R. Singla, J. Thakur, A.H. Reshak, Magnetism and magnetocrystalline anisotropy of tetragonally distorted L10-FeNi: N alloy, J. Alloys Compd. 835 (2020) 155325.